Received: 23 April 2021 | Revised: 6 June 2021 | Accepted: 20 June 2021

DOI: 10.1002/mdp2.257

REPORT

WILEY

Correlation between as-designed and as-built Young's modulus of cubic regular, cubic irregular, and trabecular cellular materials

Sunil Raghavendra[1] | **Alberto Molinari**[1] | **Gianluca Zappini**[2] | **Matteo Benedetti**[1]

[1]Department of Industrial Engineering, University of Trento, Trento, Italy

[2]Lincotek Additive, Lincotek, Pergine Valsugana, Italy

Correspondence
Sunil Raghavendra, Department of Industrial Engineering, University of Trento, Via Sommarive 9, 38123 Trento, Italy.
Email: sunil.raghavendra@unitn.it

Abstract

Laser powder bed fusion process is widely used in producing cellular materials for various applications. However, there are limitations in the process to produce high-porosity cellular materials with accuracy. A deviation is observed between the as-built and the as-designed geometrical parameters that lead to variation in the obtained stiffness of the cellular material. This study investigates the behavior of three cell topologies, cubic regular, cubic irregular, and trabecular under as-designed and as-built configurations to study their Young's modulus variation. The obtained results are compared with the ideal predictions of the Gibson–Ashby law to evaluate the deviation. Eventually, a linear correlation was developed between the as-designed and as-built Young's modulus to generate a database to select the as-designed geometry/properties to obtain the required as-built geometry/properties.

KEYWORDS

additive manufacturing, cellular material, Young's modulus

1 | INTRODUCTION

Cellular materials have proved to be a promising replacement for solid structures in applications that demand high strength-to-weight ratio. Their properties are dependent on the base material as well as the cell topology.[1] Additive manufacturing (AM) process such as laser powder bed fusion (L-PBF) has been widely used to develop and study complex and intricate shaped cellular materials ranging from simple cubic lattice-based cellular materials to gyroid-based and auxetic-based cellular materials.[2–4] L-PBF process produces specimens with better accuracy when compared to other AM processes used for metals.[5] Various studies have been carried out to characterize these cellular materials using compression, tensile, and fatigue tests to understand the effect of cell topology, relative density, and the base material.[2,6–8] Gibson–Ashby model is commonly used to theoretically predict the elastic properties of cellular materials based on their relative density. The co-efficient of the Gibson–Ashby model is dependent on the cell topology and is used to further categorize the cellular material into stretching and bending dominated cellular material.[9] A comprehensive review on the analytical relationships to predict mechanical properties of different cell topology and strut cross-sections is provided by Zadpoor and Hedayati.[10] Effects of other parameters such as Poisson's

ratio on the elastic response have also been studied for foam based cellular material.[11] All the above-mentioned studies indicate the importance of geometrical parameters such as strut thickness and cell type on the mechanical response of cellular materials.

Even though the L-PBF process can produce complex shapes, a mismatch between the as-designed and the as-built geometry is a commonly observed drawback especially in the case of cellular materials with thin struts. Studies have shown that process parameters such as scanning speed, line spacing, layer thickness, and laser power influence the melt pool during the L-PBF process, which in turn alters the final geometry of the cellular materials.[12,13] The inclination of the struts with respect to the printing direction also influences the final geometry of the struts.[14] Studies have indicated that the relation between the as-designed and the as-built strut thickness is linear in most cases. Also, the morphological deviation and geometrical defects in the strut thickness value directly influences the desired mechanical properties of cellular materials.[15] This morphological deviation must be considered while designing cellular materials, particularly for applications with tailored stiffness such as implants. One method for characterizing the morphological deviation is by relating the as-designed and as-built geometrical parameters to develop a compensated CAD model of the cell topology.[14,16] Another method to reduce the effect of mismatched geometry is by relating the as-designed and the as-built mechanical properties. This relationship can be further used to alter the as-designed relative density, and to predict the as-built mechanical properties for a given cell topology and process parameters.

In this current study, cellular materials with three different topologies, namely, cubic regular, cubic irregular, and trabecular are investigated. A total of 12 different specimens are considered for each cell topology by varying their strut thickness and pore size. A combination of finite element (FE) analysis of as-designed cellular material and experimental results of as-built configuration is used to develop an empirical relationship between their elastic moduli. This empirical relation aids in fine-tuning the as-designed relative density to obtain the desired as-built properties.

2 | MATERIALS AND METHODS

2.1 | Specimen details

The titanium alloys (Ti6Al4V) specimens were manufactured using the L-PBF process using a Renishaw AM250 laser melting machine at Lincotek, Italy. Biomedical grade titanium alloy (Ti6Al4V) powder with an average particle size between 15 and 45 μm was used for the process. A laser power of 200 W and a layer thickness of 60 μm was used for the L-PBF process. The specimens were subsequently subjected to a heat treatment according to the company internal procedure, aimed to anneal the α-martensitic as-built microstructure, transforming it into a more stable α + β lamellar structure, and to remove residual stresses. A schematic representation of the cubic regular, cubic irregular (obtained from misaligning the nodes of cubic regular), and trabecular (obtained by joining four to six struts randomly at a node) topologies are shown in Figure 1.

Twelve different specimens were obtained for each cell topology by varying their strut thickness (50, 100, and 200 μm) and pore size (700, 1000, 1500, and 2000 μm) values. The designed porosity was determined using the as-designed Computer Aided Design (CAD) model and the as-built porosity was calculated from the manufactured specimens using the methodology described in our previous work.[17]

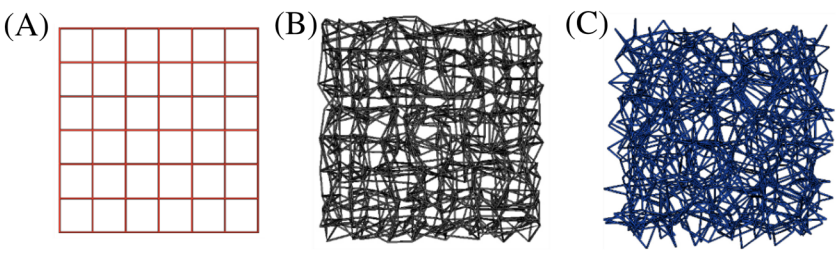

FIGURE 1 Schematic wireframe representation of cell topologies (A) cubic regular, (B) cubic irregular, and (C) trabecular

2.2 | Experimental

All the specimens were subjected to compression and tensile tests under monotonic and cyclic loading conditions. Compression test was carried out on cylindrical specimens according to ISO 13314:2011,[18] while tensile tests were carried out on specifically designed specimens with elongated cellular part attached to solid ends that act as grips for clamping into the testing machine.[7,17] Instron 8516 universal testing machine was used; the test was carried out at room temperature with a constant crosshead speed of 1 mm/min; and data sampling was carried out at a frequency of 1 kHz. The displacement under compression loading was measured using an Linear Variable Differential Transformer (LVDT) and in tension, an extensometer was used. The cyclic test is carried out between 20% and 70% of the yield load obtained from the monotonic test as discussed in our previous work.[17] Since this study focuses to obtain a relationship between the as-designed and as-built Young's modulus, the unloading Young's modulus of the cyclic test is considered. Three specimens were tested under cyclic conditions for each combination of strut thickness and pore size.

2.3 | FE analysis

FE analysis was carried out on the as-designed cellular materials to calculate Young's modulus value. The STL files from the as-designed CAD models were converted into 3D solid models using 10-noded tetrahedron elements (SOLID187). An element size of 15, 30, and 55 μm was used for strut thickness values of 50, 100, and 200 μm, respectively. A representative volume element (RVE) model was generated for all the cell specimens with at least five junctions (125 unit cells in the case of cubic regular) in each direction. The dimensions of the RVE model varied between a cube of 4 and 7 mm in each direction depending on the strut thickness and pore size. The number of elements in the FE model varied between 0.6 and 3 million depending on the RVE model and as-designed geometrical parameters. An example of the RVE models is provided in Figure A1. A displacement-based elastic analysis was carried out on the RVE model using ANSYS®. The bottom surface of the RVE model was constrained in all three directions and the top surface was fixed in *X* and *Z* directions with a vertical displacement along the vertical *Y*-direction. The stiffness obtained from the FE analysis was not influenced by the direction of loading (compression or tension); hence, the obtained modulus from the FE analysis is used to compare with the experimental values obtained from tensile as well as compression test.

3 | RESULTS AND DISCUSSION

3.1 | Young's modulus of as-designed and as-built specimens

The comparison of the relative Young's modulus and the relative density of the as-designed and as-built configuration is shown in Figure 2. The relative modulus of the specimen is obtained by using the bulk modulus of Ti6Al4V alloy (110 GPa). This relationship provides a better understanding of the mechanical behavior of the analyzed cell topologies, as per the predictions from the Gibson–Ashby model.[9] The Gibson–Ashby model is shown in Equation 1; where *C* is the Gibson–Ashby constant, the value of which depends on the cell topology and *n* is the exponent.

$$\frac{E}{E0} = \mathrm{C}\left(\frac{\rho}{\rho 0}\right)n. \tag{1}$$

The curves for the as-designed configuration are shown in Figure 2A, the cubic regular specimens have a slope of 1 while the cubic irregular and trabecular specimens have slopes of 1.93 and 1.87. These values are close to the ideal value of 1 and 2 of the coefficient *n* in Equation 1, indicating a purely stretching and bending dominated behavior, respectively. Similar curves are plotted for the as-built configurations of these specimens using the cyclic modulus or the unloading modulus from the tensile and compression test as shown in Figure 2B–D. A small difference between the modulus under tensile and compression loading is observed for all the cell topologies. However, the slope of the curves is similar under both the loading conditions as indicated in Table 1. The slope of cubic irregular and trabecular is higher than the ideal value of 2, and for cubic regular, it is higher than the ideal value of 1. This discrepancy in the as-built specimens can also be due to the presence of surface irregularities, unmelted powder particles attached to the surface which contribute to a higher density of the specimens but do not influence the load-bearing capacity of the specimen.[19]

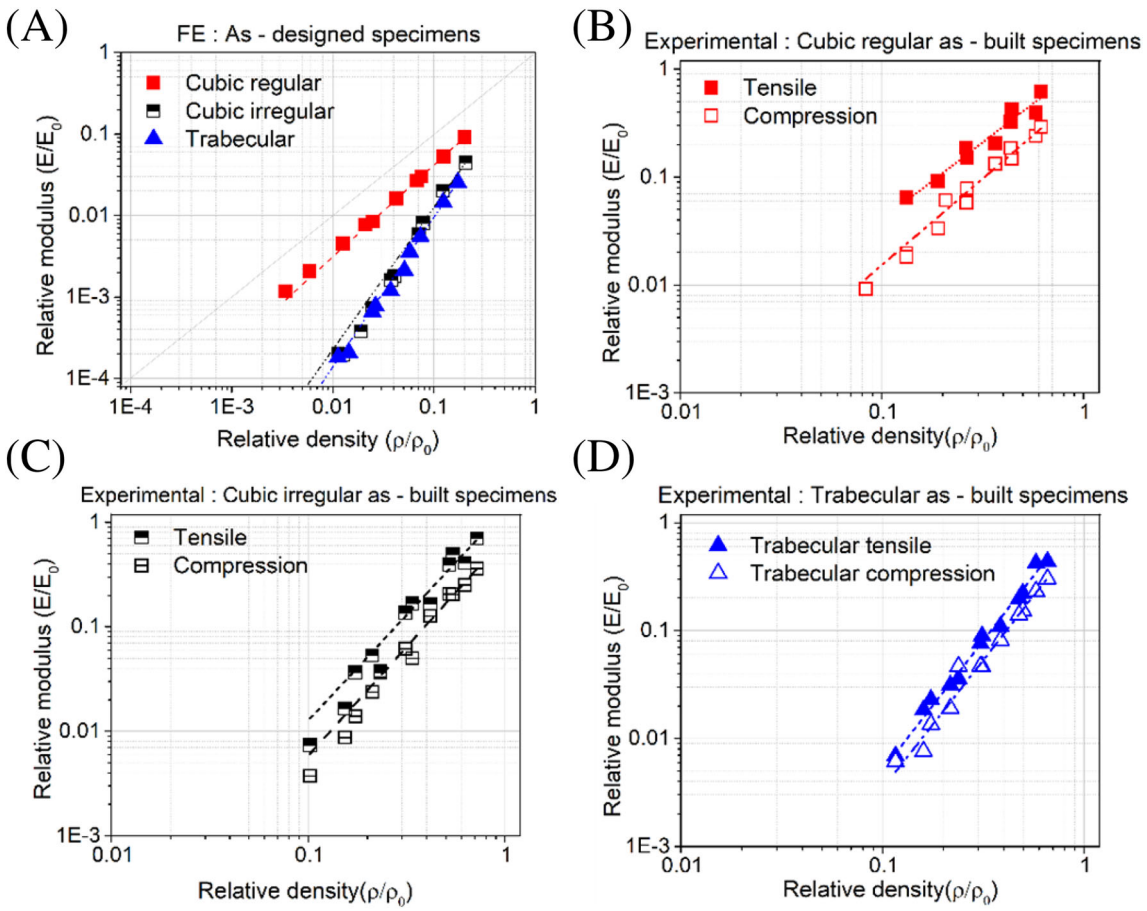

FIGURE 2 Relative density versus relative Young's modulus (A) as-designed configuration, (B) as-built cubic regular, (C) as-built cubic irregular, and (D) as-built trabecular

TABLE 1 Gibson–Ashby model coefficients for as-designed (FEM) and as-built (experimental) configuration

	As-designed FE		Compression—exp		Tensile—exp	
Sample	**C**	**n**	**C**	**n**	**C**	**n**
Cubic regular	0.5	1	0.69	1.74	1.06	1.41
Cubic irregular	0.9	1.93	0.85	2.36	1.61	2.32
Trabecular	0.67	1.87	0.79	2.34	1.07	2.18

The as-designed and the as-built porosity values are tabulated in Table A1. The coefficient *C* for all the specimens indicated in the Table 1 is between 0.1 and 4 as predicted by the Gibson–Ashby model for open-cell metallic cellular materials.[9]

3.2 | Relation between as-designed and as-built modulus

The logarithmic values of as-designed and as-built Young's modulus are plotted as shown in Figures 3 and A2 for all the cell topologies under compression and tensile loading, respectively. The correlation between the values is linear on the double log-scale plots and the curve fitting is given by Equation 2, where *A* is the slope and *B* is the intercept of the linear fitting.

$$\mathrm{Log}(\mathrm{E}_{as-built}) = \mathrm{A} \times \mathrm{Log}(\mathrm{E}_{as-designed}) + \mathrm{B}. \quad (2)$$

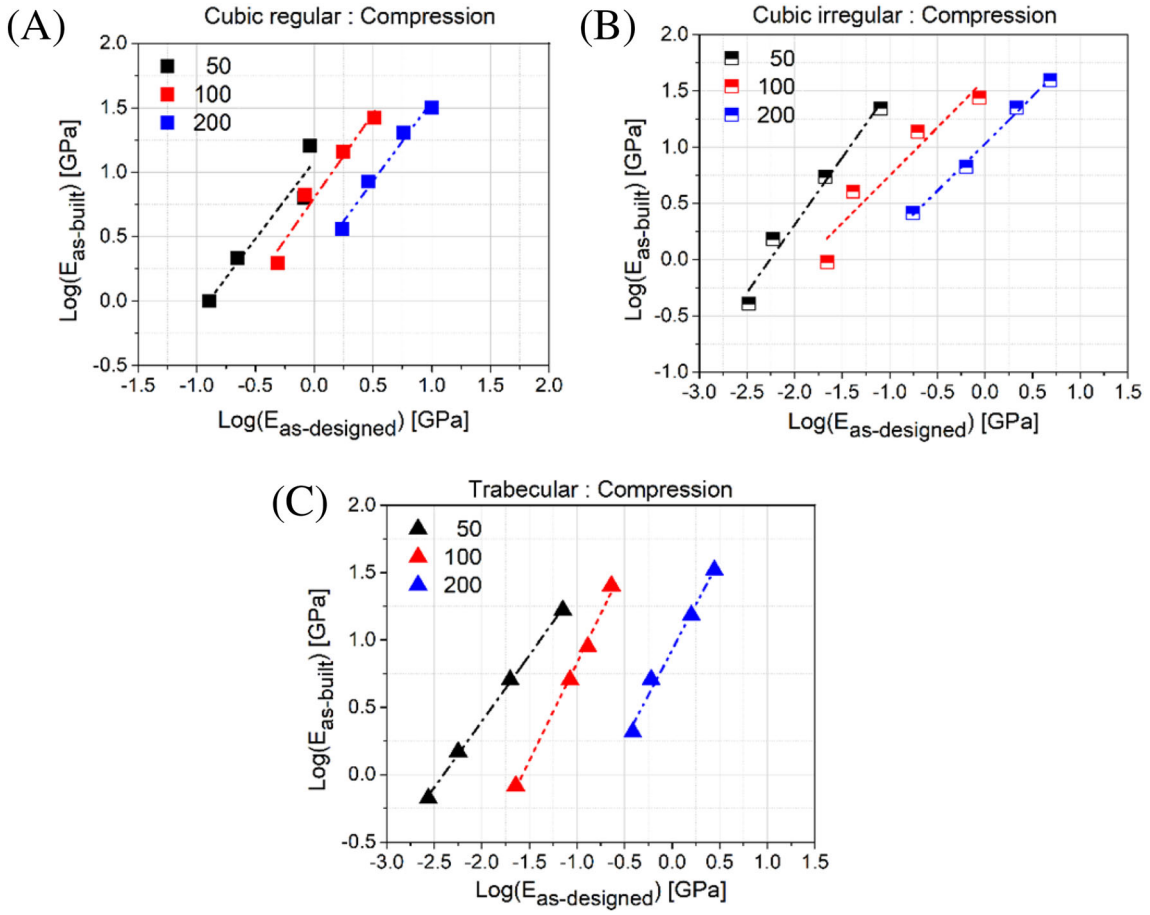

FIGURE 3 Representation of linear relation between as-designed and as-built compression modulus using a log–log scale

Figure 3 indicates that the linear relationship exhibits a clear dependency on the strut thickness of the compression test specimens for a given pore size for all cell topologies. Furthermore, from the slope and the intercept values tabulated in Table A2, it is observed that the value of the intercept decreases with a decrease in the strut thickness. Among all considered topologies and testing conditions, the data related to the cubic regular specimens under tensile loading seem to be unreliable, as shown in Figure A2A, because of the very low measured Young's modulus (subjected to high measure uncertainty) and the few data points (only two measured available). The high calculated slope (7.21) can be therefore judged as erroneous. For all the other specimens, the calculated correlations can predict the as-built Young's modulus from the as-designed Young's modulus. The obtained relationship can be effectively used for a wide range of porosity varying between 30% and 98% from as-designed as well as-built configuration, by keeping the L-PBF process parameters constant.

4 | CONCLUSION

In this current study, three different cell topologies of titanium alloy (Ti6Al4V) cellular materials with different porosities were subjected to experimental and finite element analysis to obtain the as-built and the as-designed Young's modulus, respectively. A discrepancy was observed between the as-designed and the as-built porosity of the specimens due to the L-PBF process. The results indicated that the Gibson–Ashby model works well for high-porosity specimens and deviates for low-porosity specimens. A linear relationship between the as-designed and the as-built Young's modulus was obtained for all the cell topologies that varied based on the strut thickness. This methodology can be used to estimate the as-built Young's modulus without FE analysis and to generate a database for different cell topologies for a given process parameter. It can be used to select the as-designed configuration to develop a required as-built configuration based on Young's modulus. Further experimental analysis can be used to improve this methodology to predict Young's modulus of as-built specimens directly from the design parameters.

CONFLICT OF INTEREST

The authors declared that there is no conflict of interest.

DATA AVAILABILITY STATEMENT

Research data are not shared.

ORCID

Sunil Raghavendra https://orcid.org/0000-0002-6051-2118
Matteo Benedetti https://orcid.org/0000-0001-9158-2429

REFERENCES

1. Benedetti M, du Plessis A, Ritchie RO, Dallago M, Razavi SMJ, Berto F. Architected cellular materials: a review on their mechanical properties towards fatigue-tolerant design and fabrication. *Mater Sci Eng R Rep*. 2021;144:1-40.
2. Ahmadi SM, Yavari SA, Wauthle R, et al. Additively manufactured open-cell porous biomaterials made from six different space-filling unit cells: the mechanical and morphological properties. *Materials (Basel)*. 2015;8(4):1871-1896.
3. Bobbert FSL, Lietaert K, Eftekhari AA, et al. Additively manufactured metallic porous biomaterials based on minimal surfaces: a unique combination of topological, mechanical, and mass transport properties. *Acta Biomater*. 2017;53:572-584.
4. Kolken HMA, Janbaz S, Leeflang SMA, Lietaert K, Weinans HH, Zadpoor AA. Rationally designed meta-implants: a combination of auxetic and conventional meta-biomaterials. *Materials Horizons*. 2018;5(1):28-35.
5. Tan XP, Tan YJ, Chow CSL, Tor SB, Yeong WY. Metallic powder-bed based 3D printing of cellular scaffolds for orthopaedic implants: a state-of-the-art review on manufacturing, topological design, mechanical properties and biocompatibility. *Mater Sci Eng C*. 2017;76:1328-1343.
6. Amin Yavari S, Ahmadi SMM, Wauthle R, et al. Relationship between unit cell type and porosity and the fatigue behavior of selective laser melted meta-biomaterials. *J Mech Behav Biomed Mater*. 2015;43:91-100.
7. Köhnen P, Haase C, Bültmann J, Ziegler S, Schleifenbaum JH, Bleck W. Mechanical properties and deformation behavior of additively manufactured lattice structures of stainless steel. *Mater Des*. 2018;145:205-217.
8. Kováčik J, Jerz J, Mináriková N, et al. Scaling of compression strength in disordered solids: metallic foams. *Frat Ed Integrita Strutt*. 2016;10(36):55-62.
9. Gibson LJ, Ashby MF. *Cellular Solids*. Second ed. Cambridge University Press. Epub ahead of print 1 May 1997. https://doi.org/10.1017/CBO9781139878326
10. Zadpoor AA, Hedayati R. Analytical relationships for prediction of the mechanical properties of additively manufactured porous biomaterials. *J Biomed Mater Res - Part a*. 2016;104(12):3164-3174.
11. Kováčik J, Marsavina L, Linul E. Poisson's ratio of closed-cell aluminium foams. *Materials (Basel)*. 2018;11:1-11.
12. Qiu C, Yue S, Adkins NJE, et al. Influence of processing conditions on strut structure and compressive properties of cellular lattice structures fabricated by selective laser melting. *Mater Sci Eng A*. 2015;628:188-197.
13. Dong G, Tang Y, Zhao YF. A survey of modeling of lattice structures fabricated by additive manufacturing. *J Mech Des*. 139(10):1-13. Epub ahead of print 1 October 2017. https://doi.org/10.1115/1.4037305
14. Bagheri ZS, Melancon D, Liu L, Johnston RB, Pasini D. Compensation strategy to reduce geometry and mechanics mismatches in porous biomaterials built with selective laser melting. *J Mech Behav Biomed Mater*. 2017;70:17-27.
15. Liu L, Kamm P, García-Moreno F, Banhart J, Pasini D. Elastic and failure response of imperfect three-dimensional metallic lattices: the role of geometric defects induced by selective laser melting. *Journal of the Mechanics and Physics of Solids*. 2017;107:160-184.
16. Dallago M, Raghavendra S, Luchin V, et al. Geometric assessment of lattice materials built via selective laser melting. *Materials Today: Proceedings*. 2019;7(1):353-361.
17. Raghavendra S, Molinari A, Fontanari V, et al. Tension-compression asymmetric mechanical behaviour of lattice cellular structures produced by selective laser melting. *Proc Inst Mech Eng Part C J Mech Eng Sci*. 2020;234(16):3241-3256.
18. ISO 13314. ISO 13314 mechanical testing of metals, ductility testing, compression test for porous and cellular metals. Ref number ISO 2011; 133 14: 1-7.
19. Maconachie T, Leary M, Lozanovski B, et al. SLM lattice structures: properties, performance, applications and challenges. *Mater Des*. 2019;183:1-18.

How to cite this article: Raghavendra S, Molinari A, Zappini G, Benedetti M. Correlation between as-designed and as-built Young's modulus of cubic regular, cubic irregular, and trabecular cellular materials. *Mat Design Process Comm*. 2021;e257. https://doi.org/10.1002/mdp2.257

APPENDIX A.

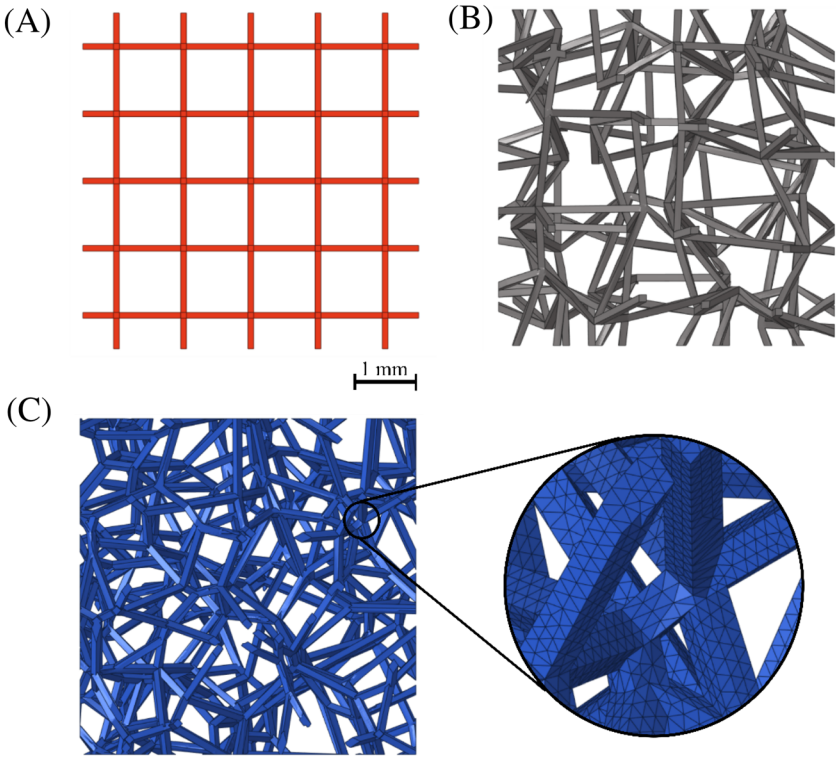

FIGURE A1 Representation of RVE model of as-designed geometry with pore size of 1500 μm and strut thickness of 100 μm (A) cubic regular, (B) cubic irregular, and (C) trabecular with a closer view of elements distribution at one of the junctions

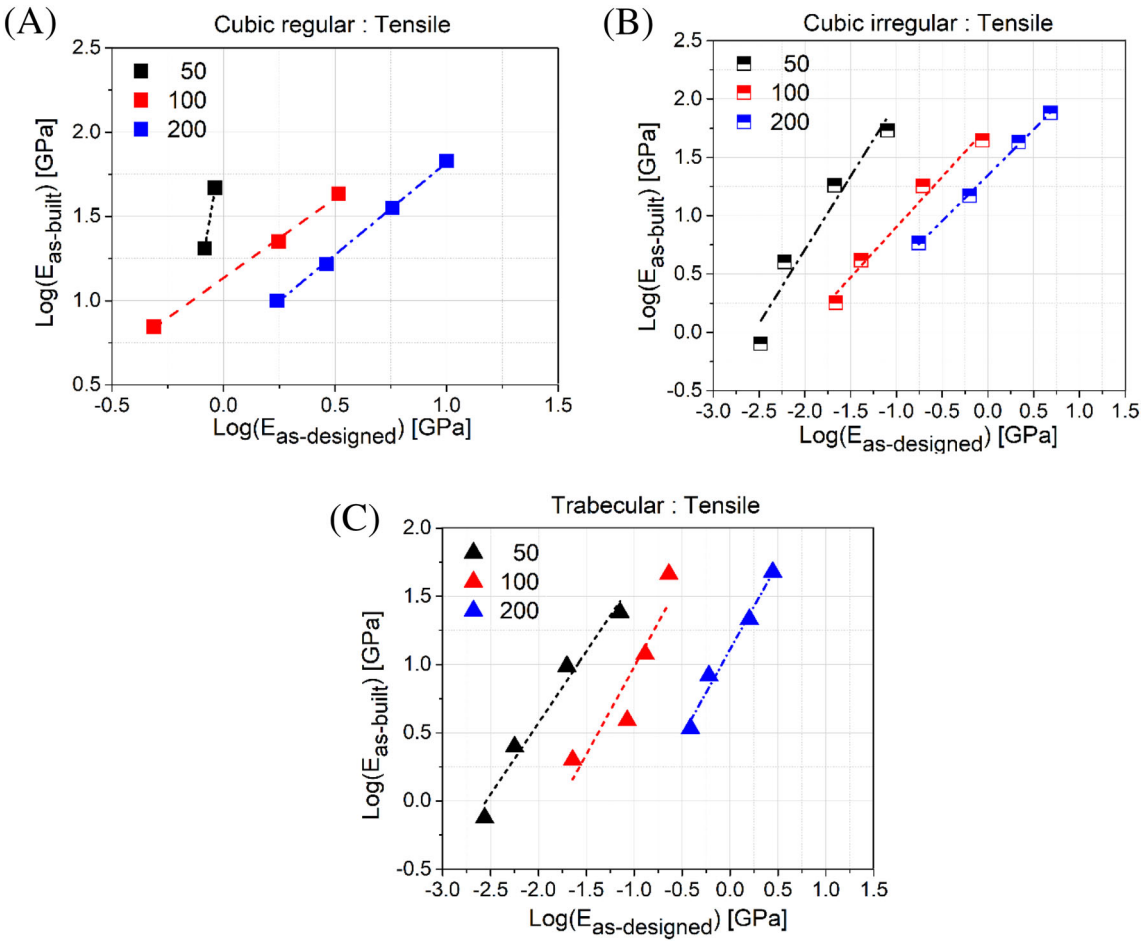

FIGURE A2 Representation of linear relation between as-designed and as-built tensile modulus using a log–log scale

TABLE A1 As-designed and as-built porosity for all cell topologies

Designed strut thickness (μm)	Designed pore size (μm)	Cubic regular porosity (%)		Cubic irregular porosity (%)		Trabecular porosity (%)	
		As-designed	As-built	As-designed	As-built	As-designed	As-built
50	700	97.5	55.9	97.5	45.6	97.5	50.2
	1000	98.8	73.8	98.7	66.2	98.9	68.8
	1500	99.4	86.8	99.4	82.6	99.3	82.6
	2000	99.7	91.7	99.6	89.8	99.6	88.4
100	700	92.5	42.1	92.2	37.5	94.9	42.2
	1000	95.8	63.5	95.9	58.2	96.3	61.5
	1500	97.9	79.3	98.1	76.7	97.4	76.1
	2000	98.8	86.8	98.9	84.6	98.6	84.0
200	700	79.9	38.5	79.3	28.0	82.8	34.1
	1000	87.6	56.5	87.7	47.9	87.6	52.3
	1500	93.3	73.6	92.9	68.8	92.7	69.3
	2000	95.8	81.0	96.2	78.8	94.2	78.3

TABLE A2 Coefficients of the linear relationship between as-designed and as-built Young's modulus

		Tensile			Compression		
Cell topology	**Strut thickness (μm)**	**A**	**B**	R^2	**A**	**B**	R^2
Cubic regular	50	(7.21)	(3.57)	—	1.72	1.50	0.92
	100	0.95	1.13	0.99	1.31	0.80	0.96
	200	1.10	0.72	0.99	1.24	0.31	0.98
Cubic irregular	50	1.61	4.00	0.95	1.34	3.02	0.98
	100	0.86	1.76	0.98	0.85	1.60	0.91
	200	0.79	1.35	1.00	0.84	1.03	1.00
Trabecular	50	1.27	3.18	0.97	1.02	2.45	0.99
	100	0.86	1.92	0.85	1.45	2.28	0.99
	200	1.26	1.11	0.98	1.34	0.93	0.98

Note: Estimation for the case "cubic regular, 50-μm strut thickness, tensile" is deemed to be not reliable due to measurement uncertainty.